Enhancing Potential of Trimethylamine Oxide on Atmospheric Particle Formation

Myllys, Nanna

2020-01

Myllys , N , Ponkkonen , T , Chee , S & Smith , J 2020 , ' Enhancing Potential of Trimethylamine Oxide on Atmospheric Particle Formation ' , Atmosphere , vol. 11 , no. 1 , 35 . https://doi.org/10.3390/atmos11010035

http://hdl.handle.net/10138/326152
https://doi.org/10.3390/atmos11010035

atmosphere

MDPI

Article

Enhancing Potential of Trimethylamine Oxide on Atmospheric Particle Formation

Nanna Myllys [1,*], Tuomo Ponkkonen [2], Sabrina Chee [1] and James Smith [1]

[1] Department of Chemistry, University of California, Irvine, CA 92697, USA; schee@uci.edu (S.C.); jimsmith@uci.edu (J.S.)

[2] Institute for Atmospheric and Earth System Research, University of Helsinki, 00014 Helsinki, Finland; tuomo.ponkkonen@gmail.com

* Correspondence: nanna.myllys@uci.edu; Tel.: +358-503-812-141

Received: 28 November 2019; Accepted: 21 December 2019; Published: 27 December 2019

Abstract: The role of an oxidation product of trimethylamine, trimethylamine oxide, in atmospheric particle formation is studied using quantum chemical methods and cluster formation simulations. Molecular-level cluster formation mechanisms are resolved, and theoretical results on particle formation are confirmed with mass spectrometer measurements. Trimethylamine oxide is capable of forming only one hydrogen bond with sulfuric acid, but unlike amines, trimethylamine oxide can form stable clusters via ion–dipole interactions. That is because of its zwitterionic structure, which causes a high dipole moment. Cluster growth occurs close to the acid:base ratio of 1:1, which is the same as for other monoprotic bases. Enhancement potential of trimethylamine oxide in particle formation is much higher than that of dimethylamine, but lower compared to guanidine. Therefore, at relatively low concentrations and high temperatures, guanidine and trimethylamine oxide may dominate particle formation events over amines.

Keywords: trimethylamine oxide; sulfuric acid; particle formation; intermolecular interactions

Key Contribution: Trimethylamine oxide enhances sulfuric acid-driven particle formation more than dimethylamine. Ion–dipole interactions may play a major role in stabilizing cluster structures in the atmosphere.

1. Introduction

Atmospheric aerosol particles are known to affect human health, and they remain to be one of the leading uncertainties in global climate modeling and predictions of future climate. A large fraction of atmospheric particles form via gas-to-particle conversion, where sulfuric acid has been shown to be a key compound in various environments [1]. Atmospheric bases such as ammonia and amines enhance sulfuric acid-driven particle formation in the lower troposphere via hydrogen-bond formation and proton-transfer reactions. Ammonia has been extensively studied since it is the most abundant base in the atmosphere at concentrations of ppb_V [2,3]. Amines have many biogenic and anthropogenic sources including animal husbandry, biomass burning, vehicle exhaust, industry, soils, and marine environments [4]. Alkylamines are the most common amines in the atmosphere, and the effect of methylamine (MA), dimethylamine (DMA) and trimethylamine (TMA) in particle formation has been investigated in many field, laboratory, and computational studies [5–15]. Both experimental and theoretical studies have concluded that in sulfuric acid-driven particle formation, the enhancing effect of the bases increases from ammonia, to MA, and finally the strongest enhancers: DMA and TMA [16–18]. While the role of amines in enhancing atmospheric cluster formation has been commonly studied, the role of the oxidized amines in particle formation and growth has received less attention.

Since the Earth's atmosphere is oxidizing, amines are subject to oxidation, thus leading to oxidation products that might have significantly different roles than amines in particle formation and growth processes [19–22].

Approximately 150 amines have been detected in the atmosphere. This, when combined with multiple oxidation pathways, results in an intractable number of possible amine oxidation products [23,24]. Here we focus on one possible oxidation product of one of the most abundant amines in the atmosphere, trimethylamine, which exists at ppt_V concentrations [24]. It is well-known that tertiary alkylamines can be oxidized readily through a number of different pathways to trialkylamine-N-oxides, or simply amine oxides [25–27]. Indeed, Angelino et al. found, for the first time in 2001, evidence of amine oxides in the particle phase [28]. They showed that trimethylamine oxide (TMAO) and triethylamine oxide (TEAO) form in the smog chamber from trimethylamine and triethylamine photooxidation processes, respectively. Since then, it has been discussed that secondary oxidation chemistry might have a larger role than acid–base reactions as a source of new particles from alkylamine precursors [29,30]. The oxidation of tertiary amines to alkylamine-N-oxides may occur in the presence of common atmospheric oxidizing agents such as ozone, oxygen radicals, hydrogen peroxide, alkylperoxy radicals, and peracids [28–31].

In addition to atmospheric oxidation processes, amine oxides might also be emitted directly into the atmosphere. TMAO is a significant nitrogen source for marine bacteria and it has been detected at nanomolar concentrations in oceanic surface waters [32,33]. Thus it is likely that TMAO is capable of participating in particle formation and growth processes in marine environments. TMAO is a common metabolite in animals and humans and, as urine contains large quantities of TMAO, animal husbandry may be a significant source for agricultural TMAO emissions [34]. TMAO is also commonly used in various industrial processes such as in pharmaceutical production and food processing [35–37].

Using high-level quantum chemical methods, we study the thermodynamics and structures of clusters containing TMAO and sulfuric acid (SA) molecules. The quantum chemical data is applied in the Atmospheric Cluster Dynamic Code (ACDC) [38] to simulate cluster population dynamics, which provide information on the enhancing role of TMAO in the form of quantities that can be measured or directly applied in atmospheric particle formation modeling. We investigate the step-by-step particle formation pathways, nanoparticle formation rates, dimer concentrations, and cluster distributions in a range of ambient conditions relevant to the lower troposphere to gain a better understanding of the enhancing effect of TMAO in atmospheric particle formation. In addition, gas-phase sulfuric acid was reacted with TMAO to observe if particles were generated in order to test if these modeling results correlated to laboratory observations of particle formation and growth. When particles did form, their composition was measured using a thermal desorption chemical ionization mass spectrometer (TDCIMS) [39] to confirm that particles grew from the reactive uptake of sulfuric acid and TMAO.

2. Methods

We studied SA–TMAO clusters containing up to 4 sulfuric acid and 4 trimethylamine oxide molecules, referred to as 4SA4TMAO. To find the global minimum energy cluster structures, we explored the potential energy surface of all the acid–base clusters using a recently developed methodology, which is tested and described in details for sulfuric acid–guanidine systems [40]. Briefly, we created all possible monomer structures of which the cluster is composed of (neutral sulfuric acid in trans or cis configuration, bisulfate, sulfate, trimethylamine oxide, and protonated trimethylamine oxide). These building blocks are used as an input in ABCluster program, which uses molecular mechanics for energy description and Artificial Bee Colony algorithm for exploring multidimensional spaces [41–43].

To create the initial cluster structures, we used 5000 random guesses and 100 exploration loops, with a scout limit of 4 in the ABCluster program, and for each building block combination we saved 500 of the lowest energy structures that were subsequently optimized by the tight-binding method GFN2-*x*TB with a very tight optimization criteria [44]. Based on the electronic energies, radius of

gyration, and dipole moments, we separated different conformers, which were then optimized using the ωB97X-D/6-31+G* level of theory [45,46]. Based on the obtained electronic energies, we selected structures with a maximum of N kcal/mol from the lowest electronic energy (where N is the number of molecules in the cluster). For remaining structures, the ωB97X-D/6-31++G** level of theory was used for final optimization and vibrational frequency calculation [47]. We selected 2–5 of the lowest Gibbs free energy structures, for which we performed single point energy calculations using the highly accurate DLPNO–CCSD(T)/aug-cc-pVTZ level of theory with tight pair natural orbital criteria, tight self consistent field criteria, and integration grid 4 [48–52]. For each clusters we identified the global minimum Gibbs free energy structure at the DLPNO–CCSD(T)/aug-cc-pVTZ//ωB97X-D/6-31++G** level [53]. The Gibbs free binding energies were calculated as:

$$\Delta G = G_{\text{cluster}} - \sum_i G_{\text{monomers},i}, \quad (1)$$

were further used to simulate step-by-step cluster formation pathways, steady-state cluster distributions, dimer concentrations, and nanoparticle formation rates.

Density functional theory calculations were done using Gaussian 16 RevA.03 [54]. Coupled cluster electronic energy corrections were calculated in Orca version 4.2.0 [55]. Cluster kinetics and population dynamics simulations were performed using Atmospheric Cluster Dynamics Code (ACDC) [38]. All the Gibbs free binding energies, enthalpies, and entropies for the minimum energy clusters, as well as the structures in the xyz format are available in the Supplementary Materials. The thermochemistry was calculated using the rigid rotor–harmonic oscillator approximation and Gibbs free energies are presented in kcal/mol and at 298.15 K unless otherwise noted. The ACDC code is available from the authors upon request.

Production of SA-TMAO Particles and Measurement with TDCIMS

Gaseous sulfuric acid was introduced into a 5 L glass reaction flask at room temperature by flowing 3.8 LPM of purified zero air (Model 737-13, Aadco Instruments) over 6 mL with 98% aqueous sulfuric acid (Fisher Scientific) held at 30 °C in a glass saturator. To start particle production, anhydrous TMAO powder (>95%, TCI Chemicals) was added directly to the reaction flask, as shown in Figure 1.

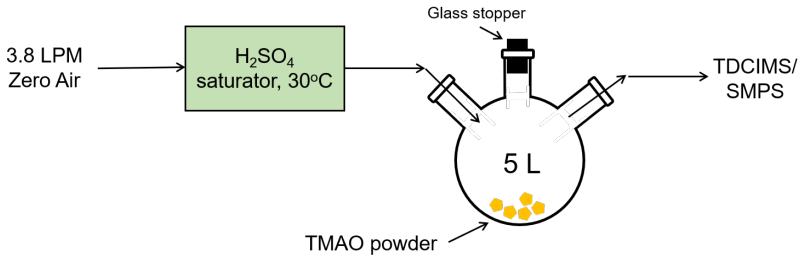

Figure 1. Particle generation setup. Generated particles were sampled directly from the reaction flask to either a nano-scanning mobility particle sizer (nano-SMPS) or the thermal desorption chemical ionization mass spectrometer (TDCIMS).

The composition of the generated particles was measured by the TDCIMS, which has been previously described in detail [39,56]. Briefly, particles were charged by a unipolar charger [57], and then size-selected by a nano-differential mobility analyzer (nano-DMA; Model 3085, TSI Inc.). The monodispersed, charged particles were then sampled by electrostatic deposition onto a Pt filament held at 3500 V during the collection process. After sufficient particulate mass was collected, the Pt filament traveled to the ionization region. The ionization region was held at 40 °C with clean N_2 flowing over the sampling orifice into the mass spectrometer in order to reduce contamination. Reagent ions were generated by a ^{210}Po radioactive source, which ionized trace amounts of oxygen and water present in the N_2 flow to make $(H_2O)_nO_2^-$ and $(H_2O)_nH_3O^+$ negative ion mode and positive ion

mode reagent ions, respectively (n = 0–2). Once in the ionization region, the Pt filament was resistively heated to volatilize particle components, wherein they were ionized and then detected by a quadrupole mass spectrometer (Extrel Corp.). Sample backgrounds were determined by repeating the same cycle without a high voltage applied to the Pt filament to prevent particle collection. In these experiments, 10 nm particles were size-selected and sampled using the TDCIMS in 1 h collection/background cycles. Particle signal was normalized to reagent ion counts to account for slight changes in reagent ion abundance. From these data, particle composition mass spectra were collected by subtracting the signal obtained from background runs from the signal obtained during collections.

Size distributions were collected with a nano-scanning mobility particle sizer (nano-SMPS), which was made up of a neutralizer containing two 0.5 mCi ^{210}Po radioactive foils (model 1U400, NRD LLC), a nano-DMA (Model 3085, TSI Inc.), and a butanol-based ultrafine particle counter (Model 3025A, TSI, Inc.) that had a 50% detection efficiency at 3 nm, as cited in the manufacturer's specifications.

3. Results and Discussion

In this section we will study the enhancing effect of trimethylamine oxide in sulfuric acid-driven particle formation and compare the results with our previous studies of guanidine (GUA) and dimethylamine (DMA) enhanced particle formation [58,59].

3.1. Acid–Base Heterodimer Stability

The stability of the acid–base heterodimer has been shown to have a major role on its ability to form larger particles at atmospheric conditions [59,60]. This means that if the heterodimer is likely to break down easily, further growth is limited. Here we compare the stability of sulfuric acid–trimethylamine oxide (1SA1TMAO) with previously studied sulfuric acid heterodimers with guanidine (1SA1GUA) and dimethylamine (1SA1DMA). In all heterodimers, the proton has transferred from sulfuric acid to base (see Figure 2). While GUA and DMA are capable of forming two hydrogen bonds, TMAO can only form one due to three methyl groups in its structure. However, the Gibbs free energy for the formation of 1SA1TMAO is the most negative, meaning it is the most stable heterodimer, with a value of −21.8 kcal/mol at 298.15 K compared to −20.3 and −13.5 kcal/mol for 1SA1GUA and 1SA1DMA, respectively. This leads to heterodimer evaporation rates of 10^{-6} s^{-3} for 1SA1TMAO, 10^{-5} s^{-3} for 1SA1GUA, and 3 s^{-3} for 1SA1DMA.

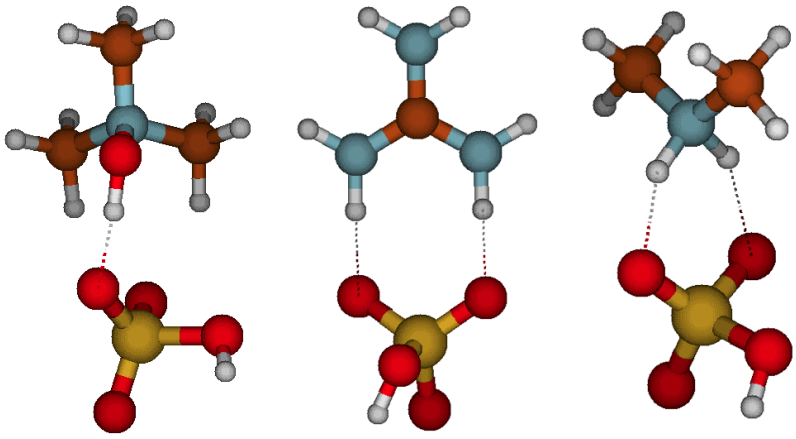

Figure 2. Molecular structures of sulfuric acid heterodimers with trimethylamine oxide (TMAO) (**left**), guanidine (GUA) (**middle**), and dimethylamine (DMA) (**right**). Color coding: Brown is carbon, blue is nitrogen, red is oxygen, yellow is sulfur, and white is hydrogen.

The reason for such a strong interaction of the one hydrogen-bond containing TMAO–SA heterodimer is related to the structure of TMAO. TMAO contains three methyl groups and a very polar zwitterionic bond, N^+–O^-. Strongly electronegative oxygen atom pulls electron density primary from

the nitrogen atom, and as a cascade reaction nitrogen atom pulls electron density from the methyl groups. This leads to a very high molecular dipole moment with a value of 5.4 D. As a consequence, the TMAO molecule is able to form strong dipole–dipole and ion–dipole interactions with surrounding molecules and ions. The dipole moment for DMA and GUA are much lower, 1.1 and 3.0 D, respectively. The absence of strong polar intramolecular bonds in DMA explains why its methyl groups do not contribute much to the molecular dipole moment, and act mostly as a steric hindrance that limits cluster formation. It should be noted that even though the TMAO molecule is a zwitterion, it is not a multi-resonance structure, meaning that single-reference quantum chemical methods can be used in this study.

3.2. Cluster Growth Pathways

At atmospherically relevant conditions, sulfuric acid–trimethylamine oxide cluster formation begins via the 1SA1TMAO cluster, since SA or TMAO homodimer formation reactions are not competitive (ΔG is -6.8 and -3.5 kcal/mol, respectively). The addition of a second TMAO or SA molecule to the 1SA1TMAO cluster is favorable with a Gibbs free reaction energy of -12.3 or -15.5 kcal/mol, respectively, indicating that the growth via 2SA1TMAO is thermodynamically more favorable. The next step is the formation of 2SA2TMAO cluster from either 1SA2TMAO or 2SA1TMAO, for which the Gibbs free reaction energy is lower than -20 kcal/mol in both cases. Additionally, the collision of two heterodimers resulting the formation of 2SA2TMAO is favorable by -14.0 kcal/mol, meaning that this reaction might be competitive with SA and TMAO additions at some conditions.

The next addition of a TMAO or SA molecule to the 2SA2TMAO cluster is thermodynamically favorable by -15.1 or -18.2 kcal/mol, respectively. This again implies the growth via 3SA2TMAO to be slightly more favorable. The formation of 3SA3TMAO from either 2SA3TMAO or 3SA2TMAO is highly favorable in both cases, with reaction free energy lower than -20 kcal/mol. The 3SA3TMAO cluster can also form as an addition of 1SA1TMAO to the 2SA2TMAO cluster, which has a reaction free energy of -17.9 kcal/mol, indicating that this reaction pathway is competitive with SA monomeric addition. In a similar manner, the formation of 4SA4TMAO may occur via monomeric additions, for which the acidic pathway is more favorable (-20.6 kcal/mol), or via collisions of 1SA1TMAO and 3SA3TMAO or two 2SA2TMAO clusters. Interestingly, the most favorable pathway to form 4SA4TMAO is the coagulation of two 2SA2TMAO clusters with a Gibbs free energy of -22.0 kcal/mol.

The Gibbs free reaction energies give information on whether additional reactions are thermodynamically favorable, however, they do not include the effect of vapor-phase concentrations of the clustering species. To examine the molecular-level clustering mechanisms at atmospheric conditions, the main step-by-step cluster formation pathways were solved by performing ACDC simulations and tracking the growth routes from the simulation data. Figure 3 shows the main growth pathways at acid and base concentrations of 10^6 cm^{-3} and 10^7 cm^{-3}, at 298.15 K. At the same conditions, we calculated the actual vapor concentration-dependent Gibbs free energies, obtained from the quantum chemical Gibbs free binding energy and vapor concentrations through the law of mass action as:

$$\Delta G(P_1, P_2, ..., P_n) = \Delta G(P_{\text{ref}}) - k_{\text{B}} T \sum_{i=1}^{n} N_i \ln \frac{P_i}{P_{\text{ref}}}, \quad (2)$$

where P_i is partial pressure of component i in the vapor phase, N_i is the number of molecules of type i in the cluster, and n is the number of components in the cluster.

Figure 3 shows that clustering is most likely to occur close to the diagonal axis with an acid:base ratio of 1:1, meaning that the number of acid and base molecules is equal or the difference between the number of acid and base molecules is one. At lower vapor concentrations, SA–TMAO clustering occurs solely via nSAnTMAO and $(n+1)$SAnTMAO clusters while at higher vapor concentrations nSA$(n+1)$TMAO clusters also participate to the growth. In the case of dimethylamine, cluster growth occurs via diagonal and below diagonal (more acid than base molecules) clusters in both lower and higher vapor concentrations. For sulfuric acid and guanidine, the 3SA4GUA cluster is involved in the

clustering pathways while other participating clusters are in diagonal and below diagonal. The cluster growth pathways and actual Gibbs free energies for dimethylamine and guanidine containing clusters are presented in the Supplementary Materials.

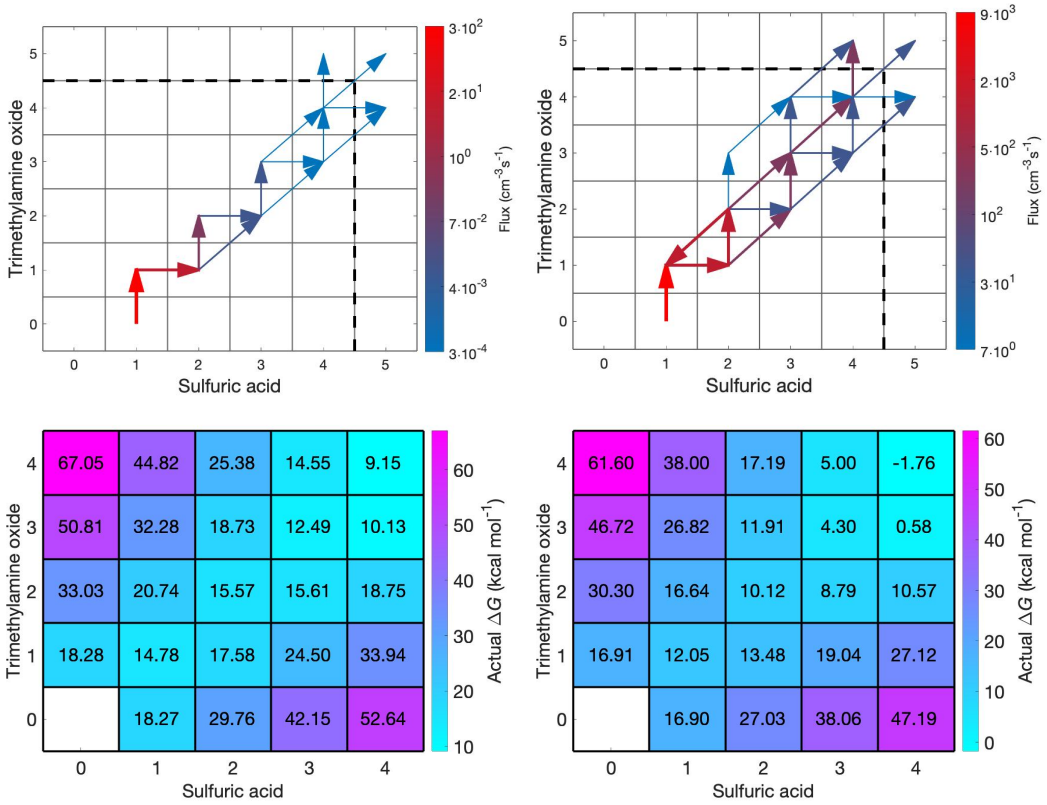

Figure 3. Main cluster growth pathways (**top**) and vapor concentration-dependent Gibbs free energies (**bottom**) for sulfuric acid (SA)–TMAO clusters at 298.15 K and vapor concentrations of [SA] = 10^6 cm^{-3} and [TMAO] = 10^6 cm^{-3} (**left**) and [SA] = 10^7 cm^{-3} and [TMAO] = 10^7 cm^{-3} (**right**). The *x*- and *y*-axes give the numbers of SA and TMAO molecules in the cluster, respectively.

Calculated vapor concentration-dependent Gibbs free energies indicate that, at lower vapor concentrations, SA–TMAO clustering occurs via a very small thermodynamic barrier involving 2SA-containing clusters. At higher concentrations there is no thermodynamic barrier and thus cluster formation is fully collision-driven. In the case of dimethylamine, there is a small barrier in both simulated conditions, whereas SA–GUA cluster formation is fully collision-driven, even at very low vapor concentrations as demonstrated in our earlier studies [58,59].

Previously, an acid:base ratio of 1:1 in the initial particle growth has been reported for other monoprotic base compounds such as methylamine, dimethylamine, and trimethylamine [16], which differs from the behavior of diprotic bases such as putresine, which has been shown to form clusters with sulfuric acid with an acid:base ratio of 2:1 [61]. While the smallest clusters of sulfuric acid and a monoprotic base are most stable at an acid:base ratio of 1:1, it has been shown that when particles reached a certain size, the acid:base ratio is 1:2, meaning fully neutralized particles where sulfuric acid has donated both protons to bases [62]. For instance, sulfuric acid and dimethylamine formed particles with an acid:base ratio of 1:2 when particle size reached 12 nm when [DMA]:[SA] = 4. In the same study, sulfuric acid and ammonia did not form fully neutralized particles smaller than 12 nm in diameter when [AMM]:[SA] = 52. Although ammonium sulfate is well-known to be a stable salt, these results imply that fully neutralized acids apply only to larger (>12 nm) sulfuric acid–ammonia particles or the amount of excess ammonia must be much larger than in studied conditions. For comparison,

monoprotic acids and bases such as nitric acid and dimethylamine are shown to form both clusters and larger particles that are fully neutralized with an acid:base ratio of 1:1 [63].

3.3. Cluster Structures, Stabilities, and Distributions

Sulfuric acid–trimethylamine oxide clustering progresses close to the 1:1 acid:base axis, because those clusters are most stable, meaning that the evaporation rates are lower compared to off-diagonal clusters (see Figure 4).

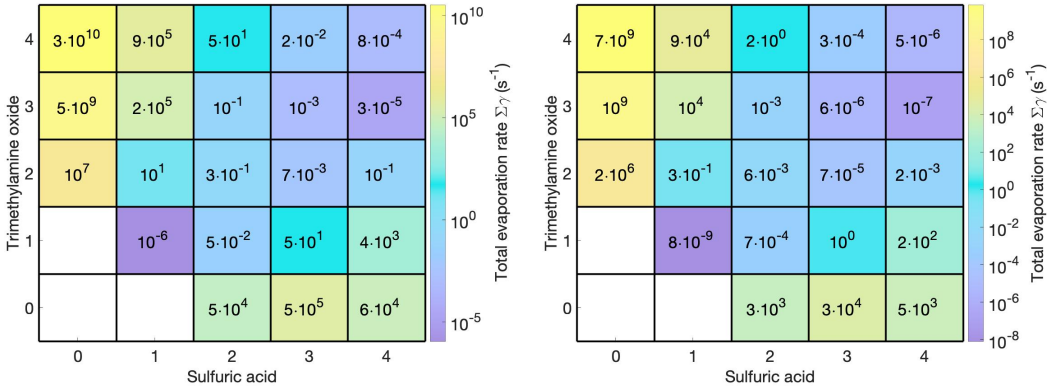

Figure 4. Overall evaporation rates of SA–TMAO clusters at 298.15 K (**left**) and 273.15 K (**right**). The *x*- and *y*-axes give the numbers of SA and TMAO molecules in the cluster, respectively.

It is notable that the SA–TMAO heterodimer has more than an order of magnitude lower evaporation rate compared to any other cluster. This seems to be relatively unique behavior compared to commonly studied acid–base clusters, including sulfuric acid with dimethylamine or guanidine for which larger close-to-diagonal clusters have at least two orders of magnitude lower evaporation rates than the heterodimer [16,59,60,63,64]. The different behavior of TMAO-containing clusters is likely due to the molecular structure of TMAO, specifically the zwitterionic N^+–O^- group with three methyl groups. Due to this unique structure, TMAO experiences a very large stabilization when interacting with a sulfuric acid monomer. Since TMAO can only form one hydrogen bond, the next interactions are either hydrogen bonds between SA molecules or ion–dipole interactions via SA and TMAO. Figure 5 shows the calculated structures of these heteroclusters.

We have simulated the steady-state SA–TMAO cluster distributions at acid and base concentrations of 10^6 and 10^7 cm^{-3}, at 298.15 K. Figure 6 shows that SA and TMAO form measurable concentrations of clusters and that nSA($n \pm 1$)TMAO clusters constitute the major fraction of the total cluster concentration. This is due to the larger stability of close-to-diagonal clusters as discussed above.

We compared the SA–TMAO cluster distributions for SA–DMA and SA–GUA distributions (see the Supplementary Materials). The cluster concentrations for SA–TMAO were significantly larger than in the case of SA–DMA. At acid and base concentrations of 10^6 cm^{-3}, only 1SA1DMA and 2SA1DMA were visible in the cluster distribution at concentrations of ca. 100 cm^{-3}. In the case of guanidine, there was the same amount of different clusters visible in the distribution, but the concentration of GUA-containing clusters was larger than that of TMAO-containing clusters. This indicates that out of the three bases, GUA was the strongest stabilizer of sulfuric acid–base clusters, TMAO was the next strongest, and DMA was the weakest.

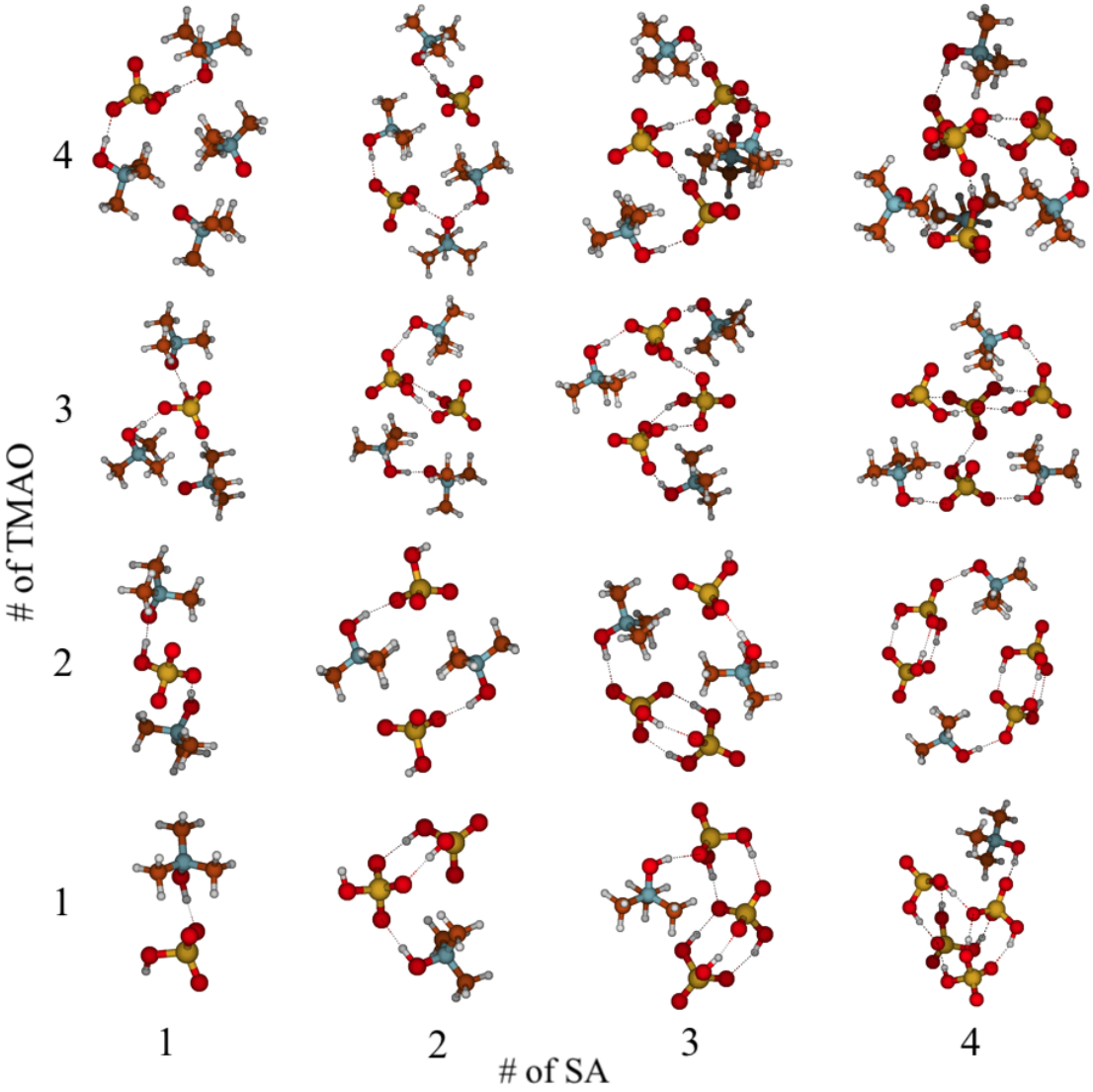

Figure 5. Molecular structures of sulfuric acid–trimethylamine oxide clusters. Color coding: Brown is carbon, blue is nitrogen, red is oxygen, yellow is sulfur, and white is hydrogen.

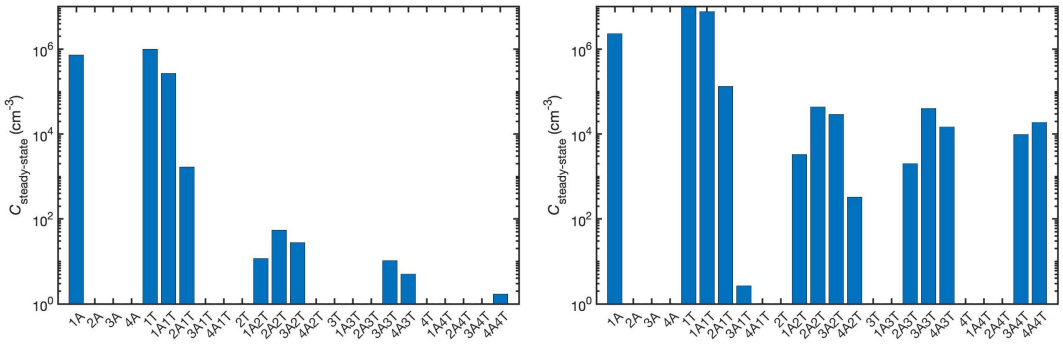

Figure 6. Steady-state cluster distributions for SA–TMAO clusters at 298.15 K and vapor concentrations of [SA] = 10^6 cm^{-3} and [TMAO] = 10^6 cm^{-3} (**left**) and [SA] = 10^7 cm^{-3} and [TMAO] = 10^7 cm^{-3} (**right**). Here A refers to sulfuric acid and T is trimethylamine oxide.

3.4. Particles Generated from SA and TMAO

By using high-level quantum chemical methods together with dynamics simulations, we can obtain molecular-level information for clusters up to ca. 1.5 nm size. We supplement these calculations with laboratory experiments in order to confirm the formation of larger particles.

Indeed, the interactions between TMAO and SA were sufficient to nucleate a large amount of particles in the laboratory. Prior to the addition of TMAO, particle concentrations in the reaction flask were below 100 cm^{-3}. However, once solid TMAO was added, over 10^6 cm^{-3} particles were generated immediately. The reaction time was approx. 1.3 min in the reaction flask and produced consistent concentrations of particles over time, as shown in the 24 h average size distribution in Figure 7.

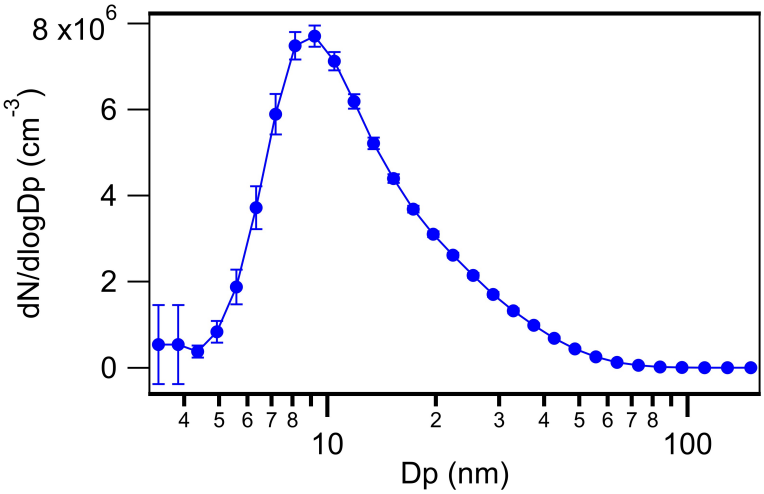

Figure 7. SA–TMAO particle number-size distribution averaged over 24 h, with error bars indicating standard deviation.

TDCIMS measurements of 10 nm particle composition show that the particles were primarily made up of sulfuric acid and TMAO (Figure 8). The major peaks in negative ion mode were decomposition products of particulate sulfate along with a nitrate contaminant (NO_2^- and NO_3^-). This nitrate signal persisted even after the inlet and particle generation apparatus had been cleaned, which reduced the abundance of these ions by an order of magnitude. The TDCIMS is known to be more sensitive to nitrate than to sulfate by as much as two orders of magnitude [65], so this ion was not expected to be a significant contributor to particle composition.

In positive ion mode, the signal from protonated TMAO (m/z 76) far exceeds that of all other detected species. It is interesting to note that protonated TMA (m/z 60) was also detected. This is most likely due to the decomposition process that occurred on the Pt filament during heating where some fraction of TMAO broke up into TMA and molecular oxygen, similar to how sulfate breaks down into SO_2^- and $(SO_3)O_2^-$, as detected in the negative ion mode spectrum.

These laboratory observations show that TMAO enhanced particle formation and growth significantly compared to sulfuric acid alone and is consistent with the model predictions that these two molecules form stable clusters.

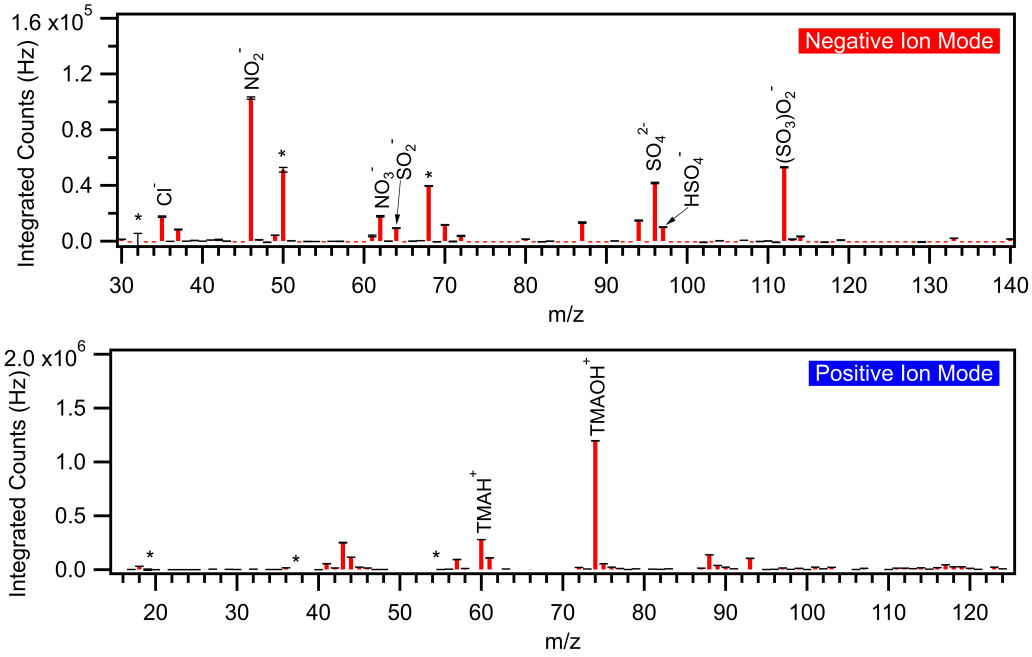

Figure 8. Background-subtracted negative and positive ion mode mass spectra of analyzed TMAO–SA particles. Asterisks (*) denote reagent ions in each spectra, which in negative ion mode are $(H_2O)_nO_2^-$, and in positive ion mode are $(H_2O)_nH_3O^+$, where n = 0–2. Negative ion mode was normalized to O_2^- (m/z 32) signal, and positive ion mode was normalized to H_3O^+ (m/z 19) signal.

3.5. Measurable Dimer Concentrations and Nanoparticle Formation Rates

We also investigated the enhancing effect of TMAO, GUA and DMA with sulfuric acid "dimers", which we define as the sum of concentrations of all clusters containing two SA molecules and any number of base molecules, i.e., ∑[2SAnBase], where n = 0–4. This quantity is also called as a measurable dimer concentration as it can be directly measured, and thus it has been used to characterize cluster formation experimentally both in laboratory and field studies [6,18,66]. In a similar manner, sulfuric acid vapor concentration is defined as the measurable "monomer" concentration, or ∑[1SAnBase]. The modeled steady-state ∑[2SAnBase] for different bases at 298.15 K as a function of ∑[1SAnBase] are presented in Figure 9.

In the case of TMAO, increasing the [TMAO] from 0.01 to 0.1 ppt_V results in an increase in the ∑[2SAnTMAO] by an order of magnitude. Higher TMAO concentrations than 0.1 ppt_V do not appreciably enhance the dimer formation, indicating that the SA–TMAO mixture reached saturation with respect to the base concentration at relatively low TMAO concentration. A similar effect can be seen in the case of guanidine. The formation of 2SAnGUA clusters is close to the saturation limit at a GUA concentration of 0.1 ppt_V and is fully reached at [GUA] = 1 ppt_V. In contrast, for the dimethylamine system at the studied vapor concentrations, every 10-fold increased in the [DMA] caused ca. 10-fold increase in the ∑[2SAnDMA]. Interestingly, while GUA had the largest enhancement in dimer formation at any acid and base concentrations, whether TMAO was more enhancing than DMA depended on the vapor concentrations. At base concentrations lower than 1 ppt_V, TMAO had a larger enhancing effect than DMA. At a base concentration of 10 ppt_V and [SA] $< 10^7$ cm^{-3}, DMA enhanced the dimer formation slightly more than TMAO, and when [SA] became higher than 10^7 cm^{-3}, the enhancing effect of TMAO was slightly larger than that of DMA.

Another quantity to determine the enhancing efficiency of base in SA-driven particle formation is the nanoparticle formation rate. We simulated the steady-state particle formation rate, which is defined as the flux of stable nanoparticles growing out from the simulated cluster size range. In the case of TMAO and GUA containing clusters, we assumed that all clusters that contain at least four acid and five base or five acid and four base are stable and in the case of DMA we considered at

least five acid and four base containing clusters to be stable nanoparticles, which were then used as boundary conditions in ACDC simulations. Simulations were performed in a range of ambient conditions relevant to the lower troposphere: At a sulfuric acid concentration range of 10^5–10^8 cm^{-3}, at base mixing ratios of 0.01, 0.1, 1, and 10 ppt_V, and at temperatures of 298.15, 273.15, and 248.15 K. Figure 10 presents the simulated nanoparticle formation rates for TMAO, GUA, and DMA containing clusters.

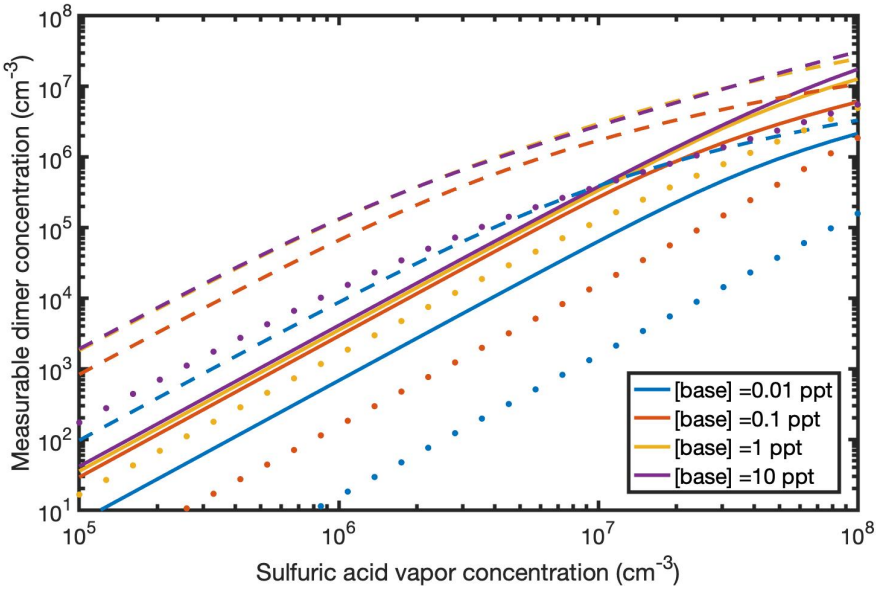

Figure 9. Steady-state concentrations of SA dimers with TMAO (solid lines), GUA (dashed lines), and DMA (dots) as a function of SA monomer concentration at 298.15 K. Note: 1 $ppt_V = 2.46 \times 10^7$ cm^{-3}.

In the TMAO-enhanced particle formation, at low SA and TMAO concentrations, a temperature decrease from 298.15 to 273.15 K resulted in up to two orders of magnitude increase in the particle formation rate. For GUA this effect was much smaller, less than an order of magnitude even at the lowest concentrations, demonstrating the very high stability of SA–GUA clusters already at room temperature. At GUA concentrations higher than 0.1 ppt_V, the effect of the decreasing temperature was negligible. In contrast, the DMA enhanced particle formation rate was increased up to five orders of magnitude at the lowest concentrations and, even at [DMA] = 10 ppt_V, the effect was three orders of magnitude, indicating relatively low stability of SA–DMA clusters. The temperature decrease from 273.15 to 248.15 K resulted in a maximum of a 10-fold increase in TMAO-enhanced and 2-fold in GUA-enhanced particle formation. On the contrary, in the case of DMA, the largest effect in simulated vapor concentrations was over 1000-fold.

In a similar manner as in modeled dimer concentrations, increasing the base concentration had a larger effect on the DMA-enhanced particle formation rate compared to the situations with TMAO and GUA. This behavior demonstrates that DMA-containing clusters were less stable, meaning more evaporation occurred compared to clusters containing TMAO and GUA. Therefore, at any modeled temperature and vapor concentrations, DMA had a lower enhancing potential compared to TMAO and GUA. Varying temperature and vapor concentrations had larger effects on TMAO than GUA enhanced particle formation. At temperatures lower than 273.15 K and at base concentrations higher than 1 ppt_V, TMAO and GUA had the same enhancement efficiency. However, in all other cases the enhancing effect of GUA was superior to TMAO at room temperature and low vapor concentrations, leading up to two orders of magnitude difference in particle formation rates.

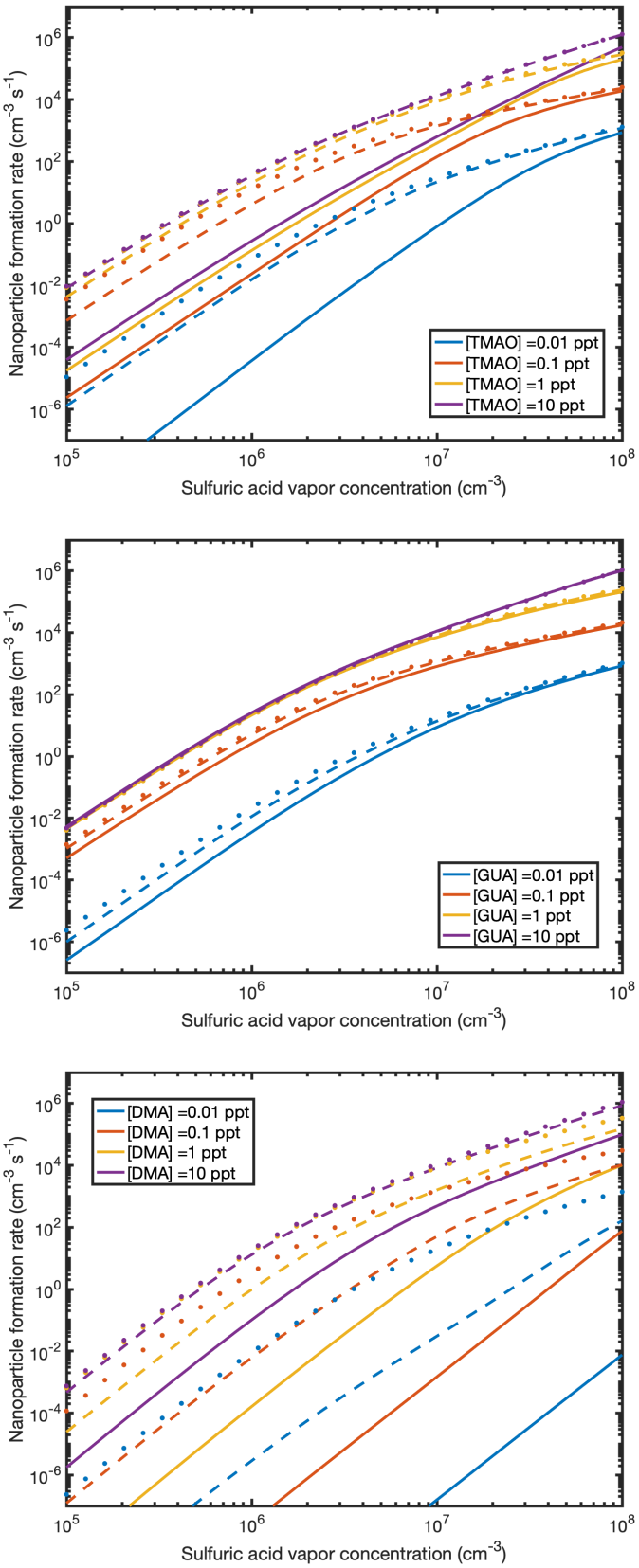

Figure 10. Nanoparticle formation rates as a function of sulfuric acid monomer concentration for TMAO (**top**), GUA (**middle**), and DMA (**bottom**). Solid lines represent T = 298.15 K, dashed lines are T = 273.15 K, and dots are T = 248 K. Note: 1 ppt_V = 2.46 × 10^7 cm^{-3}.

3.6. Base Strength and Structure versus Enhancing Potential

Base strength has been shown to be an important factor in stabilizing sulfuric acid-containing clusters thus a simplified assumption—that strong bases enhance particle formation more than weak bases—seems reasonable [59,60]. This leads to an interesting question: What factors make one base stronger than another in atmospheric particle formation? The most common definition for the strength of the Brønsted base B is the pK_b value, calculated from the equilibrium constant K_b for the reaction:

$$B + H_2O \rightarrow BH^+ + OH^- \cdot \quad \text{(R1)}$$

However, this definition assumes that the proton-transfer reaction occurs in liquid water, thus not offering the accurate representation of the base strength in a cluster. Other measures of base strength are the gas-phase basicity (GB) and proton affinity (PA) defined as a Gibbs free reaction energy and enthalpy, respectively, for the reaction in which the isolated base is taking a proton as:

$$BH^+ \rightarrow B + H^+ \cdot \quad \text{(R2)}$$

In particle formation events, however, the base molecule is interacting with other acid and base molecules, and therefore the base strength of an isolated base molecule might be significantly different than for a base molecule in a cluster. When TMAO, GUA, and DMA are in aqueous solutions, pK_b can be used to determine the base strength, where the smaller pK_b value means stronger base. In water, the order of base strengths is as follows: GUA (0.4) > DMA (3.3) > TMAO (9.3) [67]. For the isolated monomeric base molecules, the more positive the GB and PA values are, the stronger the base. In the gas-phase, the order of base strengths is the following: TMAO (227.9 kcal/mol) > GUA (226.9 kcal/mol) > DMA (214.3 kcal/mol) and the order of proton affinities is the same: TMAO (236.1 kcal/mol) > GUA (235.3 kcal/mol) > DMA (222.6 kcal/mol), calculated at the DLPNO–CCSD(T)/aug-cc-pVTZ//ωB97X-D/6-31++G** level of theory.

The findings of previous sections demonstrate that the enhancing efficiency of the studied bases follows an order of GUA > TMAO > DMA. This is very interesting, since the enhancing potential of a base in particle formation do not follow either the aqueous-phase or gas-phase base strength. The same effect has been shown for ammonia, methylamine, dimethylamine, and trimethylamine in SA-driven particle formation [7,13,16,68]. Therefore, it is of utmost importance to either develop a measure for base strength that is capable of describing aerosol particles or be able to apply the existing theories for base strength in a suitable way so as to capture the particle size- and structure-dependency.

In addition to base strength, structural effects, especially the number of hydrogen bonds, have been shown to play an important role in the initial steps of particle formation [10,13,59,61,64,68–71]. That is because hydrogen bonds, particularly between anions and cations, are very strong intermolecular interactions, thus stabilizing the cluster structure. However, as we have shown in previous sections, TMAO is capable of forming only one hydrogen bond with sulfuric acid, whereas DMA has two and GUA up to six hydrogen binding sites. Here we have demonstrated the importance of another intermolecular interaction besides hydrogen bonding: ion–dipole interactions. As shown from Figure 5, some parts of the clusters were bound without any hydrogen bonds. One interesting example is clusters containing four sulfuric acid and two base molecules. As Figure 11 shows, the 4SA2TMAO cluster contains two 2SA1TMAO parts that interact only via ion–dipole interactions, whereas in 4SA2DMA and 4SA2GUA clusters all molecules are bridging to each other via hydrogen bonds. Nonetheless, 4SA2TMAO is more stable than 4SA2DMA and 4SA2GUA clusters, having an evaporation rate of 10^{-1} s^{-1} at 298.15 K whereas the corresponding values for 4SA2DMA and 4SA2GUA are 10^3 and 8 s^{-1}, respectively. This clearly demonstrates our lack of understanding of the formation and growth mechanisms of aerosol particles.

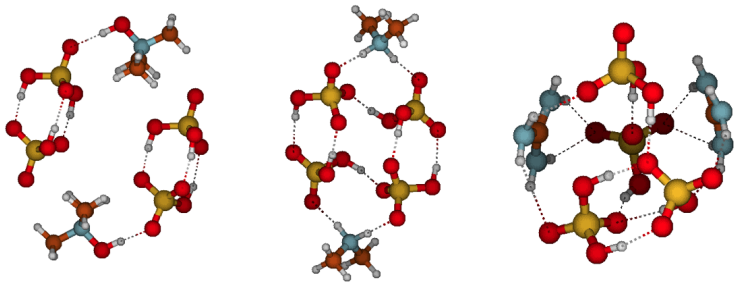

Figure 11. Molecular structures of 4SA2TMAO (**left**), 4SA2DMA (**middle**), and 4SA2GUA (**right**).

4. Conclusions

The potential role of trimethylamine oxide in atmospheric particle formation was explored. Quantum chemistry was applied to provide insights into the structures and thermodynamics of SA–TMAO clusters. Cluster kinetics and dynamics was simulated to obtain molecular-level information on the particle formation process under atmospheric conditions. We showed that TMAO largely enhanced particle formation and growth, which was further confirmed by TDCIMS measurements.

In a similar manner as other monoprotic bases, TMAO formed the most stable clusters with sulfuric acid at cluster combinations of nSA($n \pm 1$)TMAO, thus the initial growth occurred with an acid:base ratio of 1:1. In contrast to other commonly studied base compounds, the most stable SA–TMAO cluster was the heterodimer and larger clusters, which did not experience additional stabilization caused by surrounding molecules. The other interesting difference between TMAO and other base compounds containing SA clusters was that TMAO was capable of forming stable clusters, even though some parts in the clusters were interacting without hydrogen bond formation. This, as well as higher heterodimer stability, was related to the structure of TMAO. TMAO has three methyl groups and a zwitterionic N^+–O^- group, which leads to a high dipole moment and thus the capability to form strong ion–dipole interactions.

Due to the large amount of computational resources required, the effect of hydration or ions were not included in the cluster structures or molecular cluster formation simulations of this study. It has been demonstrated earlier that hydration has only a small effect in the case of dimethylamine [16], because of the small number of available hydrogen binding sites in SA–DMA cluster structures [69]. Since there is even fewer available hydrogen bonds in SA–TMAO structures, the effect of hydration is likely to be very small. While SA–GUA structures contain large number of hydrogen binding sites, those unhydrated clusters are already so stable that the enhancing effect of hydration can be expected to be small. We studied recently the enhancing effect of ions in particle formation and showed that when the main neutral cluster growth pathway contains only stable clusters, ions do not enhance particle formation efficiency [59]. Since the enhancement effect of ions were negligible for SA–GUA and at most one order of magnitude for SA–DMA, we can expect that effect to be very small in the case of SA–TMAO.

We compared the enhancing potential of TMAO with previously studied dimethylamine and guanidine compounds in SA-driven particle formation. We found that while GUA was the most effective enhancer in particle formation, the enhancing potential of TMAO was not so far away. At 298.15 K and very low (ca. 10^5 cm^{-3}) acid and base vapor concentrations, the difference in particle formation rate was two orders of magnitude. For comparison, the corresponding difference between GUA and DMA was ten orders of magnitude. Our findings showed that the enhancing potential of the studied bases followed an order of GUA > TMAO > DMA, which implies that in some environments having low vapor concentrations as well as under higher temperatures GUA and TMAO might have an enhancing role higher than DMA in SA-driven particle formation. We demonstrated that the definition of base strength in particle formation is not straightforward. As hydrogen bonding in cluster structures are commonly studied, we showed that not only hydrogen bonds but also ion–dipole interactions

can stabilize a cluster against evaporation under atmospheric conditions. Ion–dipole interactions in atmospheric particle formation are not well-studied, if at all. Thus further studies of the stabilizing role of other intermolecular interactions within clusters as well as of the concept of base strength in particle formation processes might open up new dimensions in our understanding of the formation and growth of aerosol particles and, ultimately, their impacts on air quality and climate.

Supplementary Materials: The following are available online at http://www.mdpi.com/2073-4433/11/1/35/s1, Table S1: Binding enthalpies, entropies and Gibbs free energies for all clusters; Figure S1: Main cluster growth routes of SA–GUA and SA–DMA clusters; Figure S2: Vapor concentration-dependent Gibbs free energies of SA–GUA and SA–DMA clusters; Figure S3: Steady-state cluster distributions of SA–GUA and SA–DMA clusters; zip: TMAO-containing cluster structures in xyz format.

Author Contributions: Quantum chemical calculations were performed by N.M. and T.P.; cluster formation simulations and analysis were done by N.M.; experiments were performed by S.C. and analyzed by S.C. and J.S. Manuscript preparation was done by N.M., followed by additions and suggestions given by all authors. All authors have read and agreed to the published version of the manuscript.

Funding: This research was funded by the Jenny and Antti Wihuri Foundation and the National Science Foundation grant number 1710580.

Acknowledgments: We thank the CSC-IT Center for Science in Espoo, Finland, for computational resources.

Conflicts of Interest: The authors declare no conflict of interest.

References

1. Kuang, C.; McMurry, P.H.; McCormick, A.V.; Eisele, F.L. Dependence of Nucleation Rates on Sulfuric Acid Vapor Concentration in Diverse Atmospheric Locations. *J. Geophys. Res. Atmos.* **2008**, *113*. [CrossRef]
2. Anderson, N.; Strader, R.; Davidson, C. Airborne Reduced Nitrogen: Ammonia Emissions from Agriculture and Other Sources. *Environ. Int.* **2003**, *29*, 277–286. [CrossRef]
3. Ball, S.; Hanson, D.; Eisele, F.; McMurry, P.H. Laboratory Studies of Particle Nucleation: Initial Results for H_2SO_4, H_2O, and NH_3 Vapors. *J. Geophys. Res. Atmos.* **1999**, *104*, 23709–23718. [CrossRef]
4. Cape, J.; Cornell, S.; Jickells, T.; Nemitz, E. Organic Nitrogen in the Atmosphere—Where Does It Come from? A Review of Sources and Methods. *Atmos. Res.* **2011**, *102*, 30–48. [CrossRef]
5. Kurtén, T.; Loukonen, V.; Vehkamäki, H.; Kulmala, M. Amines Are Likely to Enhance Neutral and Ion-Induced Sulfuric Acid-Water Nucleation in the Atmosphere More Effectively Than Ammonia. *Atmos. Chem. Phys.* **2008**, *8*, 4095–4103. [CrossRef]
6. Almeida, J.; Schobesberger, S.; Kürten, A.; Ortega, I.K.; Kupiainen-Määttä, O.; Praplan, A.P.; Adamov, A.; Amorim, A.; Bianchi, F.; Breitenlechner, M.; et al. Molecular Understanding of Sulphuric Acid–Amine Particle Nucleation in the Atmosphere. *Nature* **2013**, *502*, 359–363. [CrossRef]
7. Yu, H.; McGraw, R.; Lee, S.H. Effects of Amines on Formation of Sub-3 nm Particles and Their Subsequent Growth. *Geophys. Res. Lett.* **2012**, *39*, 2. [CrossRef]
8. Yao, L.; Garmash, O.; Bianchi, F.; Zheng, J.; Yan, C.; Kontkanen, J.; Junninen, H.; Mazon, S.B.; Ehn, M.; Paasonen, P.; et al. Atmospheric New Particle Formation from Sulfuric Acid and Amines in a Chinese Megacity. *Science* **2018**, *361*, 278–281. [CrossRef]
9. Erupe, M.E.; Viggiano, A.A.; Lee, S.H. The Effect of Trimethylamine on Atmospheric Nucleation Involving H_2SO_4. *Atmos. Chem. Phys.* **2011**, *11*, 4767–4775. [CrossRef]
10. Myllys, N.; Chee, S.; Olenius, T.; Lawler, M.; Smith, J.N. Molecular-Level Understanding of Synergistic Effects in Sulfuric Acid–Amine–Ammonia Mixed Clusters. *J. Phys. Chem. A* **2019**, *123*, 2420–2425. [CrossRef]
11. Kürten, A.; Jokinen, T.; Simon, M.; Sipilä, M.; Sarnela, N.; Junninen, H.; Adamov, A.; Almeida, J.; Amorim, A.; Bianchi, F.; et al. Neutral Molecular Cluster Formation of Sulfuric Acid–Dimethylamine Observed in Real Time Under Atmospheric Conditions. *Proc. Natl. Acad. Sci. USA* **2014**, *111*, 15019–15024. [CrossRef] [PubMed]
12. Paasonen, P.; Olenius, T.; Kupiainen, O.; Kurtén, T.; Petäjä, T.; Birmili, W.; Hamed, A.; Hu, M.; Huey, L.G.; Plass-Duelmer, C.; et al. On the Formation of Sulphuric Acid–Amine Clusters in Varying Atmospheric Conditions and Its Influence on Atmospheric New Particle Formation. *Atmos. Chem. Phys.* **2012**, *12*, 9113–9133. [CrossRef]

13. Temelso, B.; Morrison, E.F.; Speer, D.L.; Cao, B.C.; Appiah-Padi, N.; Kim, G.; Shields, G.C. Effect of Mixing Ammonia and Alkylamines on Sulfate Aerosol Formation. *J. Phys. Chem. A* **2018**, *122*, 1612–1622. [CrossRef] [PubMed]
14. Bustos, D.J.; Temelso, B.; Shields, G.C. Hydration of the Sulfuric Acid–Methylamine Complex and Implications for Aerosol Formation. *J. Phys. Chem. A* **2014**, *118*, 7430–7441. [CrossRef] [PubMed]
15. Hemmilä, M.; Hellén, H.; Virkkula, A.; Makkonen, U.; Praplan, A.P.; Kontkanen, J.; Ahonen, L.; Kulmala, M.; Hakola, H. Amines in Boreal Forest Air at SMEAR II Station in Finland. *Atmos. Chem. Phys.* **2018**, *18*, 6367–6380. [CrossRef]
16. Olenius, T.; Halonen, R.; Kurtén, T.; Henschel, H.; Kupiainen-Määttä, O.; Ortega, I.K.; Jen, C.N.; Vehkamäki, H.; Riipinen, I. New Particle Formation from Sulfuric Acid and Amines: Comparison of Mono-, Di-, and Trimethylamines. *J. Geophys. Res. Atmos.* **2017**, *122*, 7103–7118. [CrossRef]
17. Glasoe, W.; Volz, K.; Panta, B.; Freshour, N.; Bachman, R.; Hanson, D.; McMurry, P.; Jen, C. Sulfuric Acid Nucleation: An Experimental Study of the Effect of Seven Bases. *J. Geophys. Res. Atmos.* **2015**, *120*, 1933–1950. [CrossRef]
18. Jen, C.N.; McMurry, P.H.; Hanson, D.R. Stabilization of Sulfuric Acid Dimers by Ammonia, Methylamine, Dimethylamine, and Trimethylamine. *J. Geophys. Res. Atmos.* **2014**, *119*, 7502–7514. [CrossRef]
19. Schade, G.W.; Crutzen, P.J. Emission of Aliphatic Amines from Animal Husbandry and Their Reactions: Potential Source of N_2O and HCN. *J. Atmos. Chem.* **1995**, *22*, 319–346. [CrossRef]
20. Malloy, Q.G.J.; Qi, L.; Warren, B.; Cocker, D.R., III; Erupe, M.E.; Silva, P.J. Secondary Organic Aerosol Formation from Primary Aliphatic Amines with NO_3 Radical. *Atmos. Chem. Phys.* **2009**, *9*, 2051–2060. [CrossRef]
21. Erupe, M.E.; Liberman-Martin, A.; Silva, P.J.; Malloy, Q.G.; Yonis, N.; Cocker, D.R., III; Purvis-Roberts, K.L. Determination of Methylamines and Trimethylamine-N-oxide in Particulate Matter by Non-Suppressed Ion Chromatography. *J. Chromatogr. A* **2010**, *1217*, 2070–2073. [CrossRef] [PubMed]
22. Yu, F.; Luo, G. Modeling of Gaseous Methylamines in the Global Atmosphere: Impacts of Oxidation and Aerosol Uptake. *Atmos. Chem. Phys.* **2014**, *14*, 12455–12464. [CrossRef]
23. Ho, K.L.; Chung, Y.C.; Lin, Y.H.; Tseng, C.P. Biofiltration of Trimethylamine, Dimethylamine, and Methylamine by Immobilized Paracoccus sp. CP2 and Arthrobacter sp. CP1. *Chemosphere* **2008**, *72*, 250–256. [CrossRef] [PubMed]
24. Ge, X.; Wexler, A.S.; Clegg, S.L. Atmospheric Amines–Part I. A Review. *Atmos. Environ.* **2011**, *45*, 524–546. [CrossRef]
25. Velasquez, M.T.; Ramezani, A.; Manal, A.; Raj, D.S. Trimethylamine N-oxide: the Good, the Bad and the Unknown. *Toxins* **2016**, *8*, 326. [CrossRef]
26. Janeiro, M.H.; Ramírez, M.J.; Milagro, F.I.; Martínez, J.A.; Solas, M. Implication of Trimethylamine N-Oxide (TMAO) in Disease: Potential Biomarker or New Therapeutic Target. *Nutrients* **2018**, *10*, 1398. [CrossRef]
27. Baker, J.; Chaykin, S. The Biosynthesis of Trimethylamine-N-oxide. *J. Biol. Chem.* **1962**, *237*, 1309–1313. [CrossRef]
28. Angelino, S.; Suess, D.T.; Prather, K.A. Formation of Aerosol Particles from Reactions of Secondary and Tertiary Alkylamines: Characterization by Aerosol Time-of-Flight Mass Spectrometry. *Environ. Sci. Technol.* **2001**, *35*, 3130–3138. [CrossRef]
29. Silva, P.J.; Erupe, M.E.; Price, D.; Elias, J.; GJ Malloy, Q.; Li, Q.; Warren, B.; Cocker, D.R. Trimethylamine as Precursor to Secondary Organic Aerosol Formation via Nitrate Radical Reaction in the Atmosphere. *Environ. Sci. Technol.* **2008**, *42*, 4689–4696. [CrossRef]
30. Murphy, S.; Sorooshian, A.; Kroll, J.; Ng, N.; Chhabra, P.; Tong, C.; Surratt, J.; Knipping, E.; Flagan, R.; Seinfeld, J. Secondary Aerosol Formation from Atmospheric Reactions of Aliphatic Amines. *Atmos. Chem. Phys.* **2007**, *7*, 2313–2337. [CrossRef]
31. Atkinson, R.; Pitts, J.N. Kinetics of the Reactions of O(3P) Atoms with the Amines CH_3NH_2, $C_2H_5NH_2$, $(CH_3)_2NH$, and $(CH_3)_3N$ Over the Temperature Range 298–440 K. *J. Chem. Phys.* **1978**, *68*, 911–915. [CrossRef]
32. Lidbury, I.; Murrell, J.C.; Chen, Y. Trimethylamine N-oxide Metabolism by Abundant Marine Heterotrophic Bacteria. *Proc. Natl. Acad. Sci. USA* **2014**, *111*, 2710–2715. [CrossRef] [PubMed]

33. Li, C.Y.; Chen, X.L.; Shao, X.; Wei, T.D.; Wang, P.; Xie, B.B.; Qin, Q.L.; Zhang, X.Y.; Su, H.N.; Song, X.Y.; et al. Mechanistic Insight into Trimethylamine N-oxide Recognition by the Marine Bacterium Ruegeria Pomeroyi DSS-3. *J. Bacteriol.* **2015**, *197*, 3378–3387. [CrossRef] [PubMed]
34. Sintermann, J.; Schallhart, S.; Kajos, M.; Jocher, M.; Bracher, A.; Münger, A.; Johnson, D.; Neftel, A.; Ruuskanen, T. Trimethylamine Emissions in Animal Husbandry. *Biogeosciences* **2014**, *11*, 5073–5085. [CrossRef]
35. Knölker, H.J. Trimethylamine N-Oxide—A Useful Oxidizing Reagent. *J. Prakt. Chem. Chem. Ztg.* **1996**, *338*, 190–192. [CrossRef]
36. Åkesson, B.; Vinge, E.; Skerfving, S. Pharmacokinetics of Triethylamine and Triethylamine-N-oxide in Man. *Toxicol. Appl. Pharm.* **1989**, *100*, 529–538. [CrossRef]
37. Rappert, S.; Müller, R. Odor Compounds in Waste Gas Emissions from Agricultural Operations and Food Industries. *Waste Manag.* **2005**, *25*, 887–907. [CrossRef]
38. McGrath, M.J.; Olenius, T.; Ortega, I.K.; Loukonen, V.; Paasonen, P.; Kurtén, T.; Kulmala, M.; Vehkamäki, H. Atmospheric Cluster Dynamics Code: A Flexible Method for Solution of the Birth–Death Equations. *Atmos. Chem. Phys.* **2012**, *12*, 2345–2355. [CrossRef]
39. Voisin, D.; Smith, J.N.; Sakurai, H.; McMurry, P.; Eisele, F.L. Thermal Desorption Chemical Ionization Mass Spectrometer for Ultrafine Particle Chemical Composition. *Aerosol Sci. Technol.* **2003**, *37*, 471–475. [CrossRef]
40. Kubečka, J.; Besel, V.; Kurtén, T.; Myllys, N.; Vehkamäki, H. Configurational Sampling of Noncovalent (Atmospheric) Molecular Clusters: Sulfuric Acid and Guanidine. *J. Phys. Chem. A* **2019**, *123*, 6022–6033. [CrossRef]
41. Zhang, J.; Dolg, M. ABCluster: The Artificial Bee Colony Algorithm for Cluster Global Optimization. *Phys. Chem. Chem. Phys.* **2015**, *17*, 24173–24181. [CrossRef] [PubMed]
42. Zhang, J.; Dolg, M. Global Optimization of Clusters of Rigid Molecules using the Artificial Bee Colony Algorithm. *Phys. Chem. Chem. Phys.* **2016**, *18*, 3003–3010. [CrossRef] [PubMed]
43. Karaboga, D.; Basturk, B. On the Performance of Artificial Bee Colony (ABC) Algorithm. *Appl. Soft Comput.* **2008**, *8*, 687–697. [CrossRef]
44. Bannwarth, C.; Ehlert, S.; Grimme, S. GFN2-xTB—An Accurate and Broadly Parametrized Self-Consistent Tight-Binding Quantum Chemical Method with Multipole Electrostatics and Density-Dependent Dispersion Contributions. *J. Chem. Theory Comput.* **2019**, *15*, 1652–1671. [CrossRef]
45. Chai, J.D.; Head-Gordon, M. Long-Range Corrected Hybrid Density Functionals with Damped Atom-Atom Dispersion Corrections. *Phys. Chem. Chem. Phys.* **2008**, *10*, 6615–6620. [CrossRef]
46. Krishnan, R.; Binkley, J.S.; Seeger, R.; Pople, J.A. Self-Consistent Molecular Orbital Methods. XX. A Basis Set for Correlated Wave Functions. *J. Chem. Phys.* **1980**, *72*, 650–654. [CrossRef]
47. Myllys, N.; Elm, J.; Kurtén, T. Density Functional Theory Basis Set Convergence of Sulfuric Acid-Containing Molecular Clusters. *Comput. Theor. Chem.* **2016**, *1098*, 1–12. [CrossRef]
48. Riplinger, C.; Neese, F. An Efficient and Near Linear Scaling Pair Natural Orbital Based Local Coupled Cluster Method. *J. Chem. Phys.* **2013**, *138*, 034106. [CrossRef]
49. Riplinger, C.; Sandhoefer, B.; Hansen, A.; Neese, F. Natural Triple Excitations in Local Coupled Cluster Calculations with Pair Natural Orbitals. *J. Chem. Phys.* **2013**, *139*, 134101. [CrossRef]
50. Riplinger, C.; Pinski, P.; Becker, U.; Valeev, E.F.; Neese, F. Sparse Maps—A Systematic Infrastructure for Reduced-Scaling Electronic Structure Methods. II. Linear Scaling Domain Based Pair Natural Orbital Coupled Cluster Theory. *J. Chem. Phys.* **2016**, *144*, 024109. [CrossRef]
51. Kendall, R.A.; Dunning, T.H.; Harrison, R.J. Electron Affinities of the First-Row Atoms Revisited. Systematic Basis Sets and Wave Functions. *J. Chem. Phys.* **1992**, *96*, 6796–6806. [CrossRef]
52. Liakos, D.G.; Sparta, M.; Kesharwani, M.K.; Martin, J.M.L.; Neese, F. Exploring the Accuracy Limits of Local Pair Natural Orbital Coupled-Cluster Theory. *J. Chem. Theory Comput.* **2015**, *11*, 1525–1539. [CrossRef]
53. Myllys, N.; Elm, J.; Halonen, R.; Kurtén, T.; Vehkamäki, H. Coupled Cluster Evaluation of the Stability of Atmospheric Acid–Base Clusters with up to 10 Molecules. *J. Phys. Chem. A* **2016**, *120*, 621–630. [CrossRef] [PubMed]
54. Frisch, M.J.; Trucks, G.W.; Schlegel, H.B.; Scuseria, G.E.; Robb, M.A.; Cheeseman, J.R.; Scalmani, G.; Barone, V.; Petersson, G.A.; Nakatsuji, H.; et al. *Gaussian16 Revision A. 03*; Gaussian Inc.: Wallingford, CT, USA, 2016.
55. Neese, F. The ORCA Program System. *Wiley Interdiscip. Rev. Comput. Mol. Sci.* **2012**, *2*, 73–78. [CrossRef]

56. Smith, J.N.; Moore, K.F.; McMurry, P.H.; Eisele, F.L. Atmospheric Measurements of Sub-20 nm Diameter Particle Chemical Composition by Thermal Desorption Chemical Ionization Mass Spectrometry. *Aerosol Sci. Technol.* **2004**, *38*, 100–110. [CrossRef]
57. Chen, D.R.; Pui, D.Y. A High Efficiency, High Throughput Unipolar Aerosol Charger for Nanoparticles. *J. Nanoparticle Res.* **1999**, *1*, 115–126. [CrossRef]
58. Myllys, N.; Ponkkonen, T.; Passananti, M.; Elm, J.; Vehkamäki, H.; Olenius, T. Guanidine: A Highly Efficient Stabilizer in Atmospheric New-Particle Formation. *J. Phys. Chem. A* **2018**, *122*, 4717–4729. [CrossRef]
59. Myllys, N.; Kubečka, J.; Besel, V.; Alfaouri, D.; Olenius, T.; Smith, J.N.; Passananti, M. Role of Base Strength, Cluster Structure and Charge in Sulfuric-Acid-Driven Particle Formation. *Atmos. Chem. Phys.* **2019**, *19*, 9753–9768. [CrossRef]
60. Elm, J. Elucidating the Limiting Steps in Sulfuric Acid–Base New Particle Formation. *J. Phys. Chem. A* **2017**, *121*, 8288–8295. [CrossRef]
61. Elm, J.; Jen, C.N.; Kurtén, T.; Vehkamäki, H. Strong Hydrogen Bonded Molecular Interactions between Atmospheric Diamines and Sulfuric Acid. *J. Phys. Chem. A* **2016**, *120*, 3693–3700. [CrossRef]
62. Chen, H.; Chee, S.; Lawler, M.J.; Barsanti, K.C.; Wong, B.M.; Smith, J.N. Size Resolved Chemical Composition of Nanoparticles from Reactions of Sulfuric Acid with Ammonia and Dimethylamine. *Aerosol Sci. Technol.* **2018**, *52*, 1120–1133. [CrossRef]
63. Chee, S.; Myllys, N.; Barsanti, K.C.; Wong, B.M.; Smith, J.N. An Experimental and Modeling Study of Nanoparticle Formation and Growth from Dimethylamine and Nitric Acid. *J. Phys. Chem. A* **2019**, *123*, 5640–5648. [CrossRef] [PubMed]
64. Xie, H.B.; Elm, J.; Halonen, R.; Myllys, N.; Kurtén, T.; Kulmala, M.; Vehkamäki, H. Atmospheric Fate of Monoethanolamine: Enhancing New Particle Formation of Sulfuric Acid as an Important Removal Process. *Environ. Sci. Technol.* **2017**, *51*, 8422–8431. [CrossRef] [PubMed]
65. Lawler, M.J.; Whitehead, J.; O'Dowd, C.; Monahan, C.; McFiggans, G.; Smith, J.N. Composition of 15–85 nm Particles in Marine Air. *Atmos. Chem. Phys.* **2014**, *14*, 11557–11569. [CrossRef]
66. Kürten, A.; Bergen, A.; Heinritzi, M.; Leiminger, M.; Lorenz, V.; Piel, F.; Simon, M.; Sitals, R.; Wagner, A.C.; Curtius, J. Observation of New Particle Formation and Measurement of Sulfuric Acid, Ammonia, Amines and Highly Oxidized Organic Molecules at a Rural Site in Central Germany. *Atmos. Chem. Phys.* **2016**, *16*, 12793–12813. [CrossRef]
67. Rumble, J. *CRC Handbook of Chemistry and Physics*; CRC Press: Boca Raton, FL, USA, 2017.
68. Waller, S.E.; Yang, Y.; Castracane, E.; Racow, E.E.; Kreinbihl, J.J.; Nickson, K.A.; Johnson, C.J. The Interplay Between Hydrogen Bonding and Coulombic Forces in Determining the Structure of Sulfuric Acid-Amine Clusters. *J. Phys. Chem. Lett.* **2018**, *9*, 1216–1222. [CrossRef]
69. Yang, Y.; Waller, S.E.; Kreinbihl, J.J.; Johnson, C.J. Direct Link between Structure and Hydration in Ammonium and Aminium Bisulfate Clusters Implicated in Atmospheric New Particle Formation. *J. Phys. Chem. Lett.* **2018**, *9*, 5647–5652. [CrossRef]
70. Elm, J.; Myllys, N.; Kurtén, T. What Is Required for Highly Oxidized Molecules To Form Clusters with Sulfuric Acid? *J. Phys. Chem. A* **2017**, *121*, 4578–4587. [CrossRef]
71. Elm, J.; Fard, M.; Bilde, M.; Mikkelsen, K.V. Interaction of Glycine with Common Atmospheric Nucleation Precursors. *J. Phys. Chem. A* **2013**, *117*, 12990–12997. [CrossRef]